Global diurnal precipitation cycle in the AI model GraphCast and a 5-km unified model: challenges and opportunities

Gentile, E. S. ORCID: https://orcid.org/0000-0002-6878-5145, Hunt, K. M. R. ORCID: https://orcid.org/0000-0003-1480-3755, Tomassini, L. ORCID: https://orcid.org/0000-0003-3361-7384, Harvey, B. ORCID: https://orcid.org/0000-0002-6510-8181 and Martinez-Alvarado, O. ORCID: https://orcid.org/0000-0002-5285-0379 (2026) Global diurnal precipitation cycle in the AI model GraphCast and a 5-km unified model: challenges and opportunities. Geophysical Research Letters, 53 (9). e2025GL120961. ISSN 1944-8007 doi: 10.1029/2025GL120961 Available at https://centaur.reading.ac.uk/129678/

Geophysical Research Letters

RESEARCH LETTER
10.1029/2025GL120961

Key Points:

- GraphCast captures spatial rainfall patterns but amplifies ERA5 diurnal-cycle timing biases
- The global 5-km Unified Model improves nocturnal rainfall but triggers convection too early over the land
- Results highlight the need for hybrid AI-physics approaches to improve precipitation representation

Supporting Information:

Supporting Information may be found in the online version of this article.

Correspondence to:

E. S. Gentile,
e.gentile@reading.ac.uk

Citation:

Gentile, E. S., Hunt, K. M. R., Tomassini, L., Harvey, B., & Martinez-Alvarado, O. (2026). Global diurnal precipitation cycle in the AI model GraphCast and a 5-km Unified Model: Challenges and opportunities. *Geophysical Research Letters*, *53*, e2025GL120961. https://doi.org/10.1029/2025GL120961

Received 3 DEC 2025
Accepted 9 MAR 2026

Author Contributions:

Conceptualization: Emanuele Silvio Gentile
Data curation: Emanuele Silvio Gentile, Kieran M. R. Hunt, Lorenzo Tomassini
Formal analysis: Emanuele Silvio Gentile
Funding acquisition: Ben Harvey, Oscar Martinez-Alvarado
Investigation: Emanuele Silvio Gentile
Methodology: Emanuele Silvio Gentile, Kieran M. R. Hunt, Lorenzo Tomassini
Project administration: Emanuele Silvio Gentile
Resources: Emanuele Silvio Gentile
Software: Emanuele Silvio Gentile
Supervision: Emanuele Silvio Gentile
Validation: Emanuele Silvio Gentile
Visualization: Emanuele Silvio Gentile
Writing – original draft: Emanuele Silvio Gentile

Global Diurnal Precipitation Cycle in the AI Model GraphCast and a 5-km Unified Model: Challenges and Opportunities

Emanuele Silvio Gentile[1], Kieran M. R. Hunt[1], Lorenzo Tomassini[2,3], Ben Harvey[1], and Oscar Martinez-Alvarado[1]

[1]National Centre for Atmospheric Science, Department of Meteorology, University of Reading, Reading, UK, [2]Met Office, Exeter, UK, [3]School of Mathematics, University of Leeds, Leeds, UK

Abstract This study evaluates the ability of the AI weather forecast model GraphCast to reproduce the global diurnal cycle of boreal summer precipitation, comparing it with Integrated Multi-satellite Retrievals for GPM (IMERG) satellite observations, the ERA5 reanalysis, and an experimental global 5-km Met Office Unified Model (UM) which is convection permitting but still retains an active scale-aware parametrization. ERA5 captures large-scale rainfall patterns but exhibits a premature afternoon peak and excessively weak nocturnal precipitation over land compared to IMERG. GraphCast, while reproducing realistic mean spatial rainfall distributions, inherits, and amplifies these timing and amplitude biases, concentrating precipitation near-midday and producing very little nocturnal signal. The 5-km UM improves nocturnal precipitation across many regions but overestimates rainfall over oceans and initiates convection too early over land, likely due to the still active convective parametrization. Our analysis shows that these contrasting behaviors highlight both challenges and opportunities for improving precipitation prediction through hybrid AI-physics approaches.

Plain Language Summary Accurately simulating the daily cycle of rainfall remains a major challenge for weather and climate models. This study evaluates an AI-based weather forecast model, GraphCast, in representing the global diurnal cycle of boreal summer (June–August) precipitation. Results are compared with satellite observations, a reanalysis, and a global Met Office Unified Model (UM) simulation at 5-km resolution that allows convection to occur explicitly but still includes an approximate representation of convection active. ERA5 captures large-scale rainfall patterns but produces rain too early in the day and too little at night. GraphCast shows similar but stronger errors, with rainfall concentrated around local midday. The UM improves nocturnal rainfall in many regions but still triggers convection too early over land and overestimates rainfall over oceans. These results show that combining the physical realism of kilometer-scale models with the computational efficiency of AI could improve the simulation of precipitation processes.

1. Introduction

Precipitation is a fundamental component of Earth's hydrological and energy cycles, and accurately representing its temporal variability, particularly the diurnal cycle, is essential for improving weather prediction and climate projection (G.-Y. Yang & Slingo, 2001). The diurnal cycle arises from interactions among radiative forcing, boundary-layer dynamics, convective organization, cloud-radiation-aerosol processes, surface exchange, and mesoscale circulations, making it a stringent benchmark for model physics (Bechtold et al., 2004; Edwards et al., 2020; Jensen et al., 2022; Tao et al., 2024).

The governing mechanisms differ markedly between land and ocean. Over land, daytime heating deepens the boundary layer and triggers late-afternoon to early evening rainfall maxima (G.-Y. Yang & Slingo, 2001). Over tropical oceans, nocturnal radiative cooling and boundary-layer convergence favor early morning peaks (Fang & Du, 2022; S. Yang & Smith, 2006). Regional departures, such as the nocturnal maximum over the central United States driven by mesoscale convective systems, highlight the multiscale nature of diurnal precipitation variability (Hu et al., 2021; Nesbitt & Zipser, 2003).

Despite extensive observational and modeling efforts, the diurnal cycle remains a persistent bias in global models (Christopoulos & Schneider, 2021). General Circulation Models (GCMs, O(100 km)) with parameterized convection typically trigger rainfall too early and underestimate its amplitude over land (Curt et al., 2016; Dai, 2006),

Writing – review & editing: Emanuele Silvio Gentile, Kieran M. R. Hunt, Lorenzo Tomassini, Ben Harvey, Oscar Martinez-Alvarado

while over oceans they often weaken the nocturnal peak, reflecting insufficient coupling among surface fluxes, clouds, and large-scale circulation (Dai & Trenberth, 2004; Randall et al., 1991).

Two developments have recently transformed atmospheric modeling: global storm-resolving simulations and AI-based forecasting systems. Kilometer-scale models (Harris et al., 2020; Satoh et al., 2019; Schär et al., 2020; Stevens et al., 2019; Tomassini et al., 2023) explicitly resolve deep convection and improve diurnal timing and regional rainfall structure (Jones et al., 2023; O'Gorman et al., 2021; Takasuka et al., 2024), though amplitude and phase biases persist over Africa, the Maritime Continent, and the central United States (Berthou et al., 2019; Feng et al., 2023; Rackow et al., 2025; Zou & Zhou, 2024). Their computational cost also limits temporal coverage and operational feasibility.

At the same time, AI-based global weather models have demonstrated competitive skill, often rivaling or exceeding numerical weather prediction systems in headline metrics such as RMSE. For example, Yan et al. (2025) reported reduced short-range precipitation errors with GraphCast relative to ECMWF forecasts over and Arai et al. (2025) found improved heavy rainfall scores at medium-range lead times. However, such evaluations rely largely on aggregate error statistics, offering limited insight into process fidelity and potentially masking physical inconsistencies (Bonavita, 2024; Hunt, 2025). It therefore remains unclear whether AI models reproduce physically consistent temporal structures such as the diurnal cycle.

In this study, we evaluate the ability of the AI model GraphCast to reproduce the global diurnal precipitation cycle during boreal summer (June–August), focusing on its mean rate, amplitude, and phase. We compare GraphCast with ERA5 (Hersbach et al., 2020), the Integrated Multi-satellite Retrievals for GPM (IMERG) satellite product (Huffman et al., 2015), and a global 5 km Met Office Unified Model (UM) simulation that explicitly permits convection while retaining a scale aware parametrization (Tomassini, 2025). This process-based intercomparison assesses whether GraphCast captures the mechanisms underlying diurnal precipitation variability or primarily reproduces patterns embedded in its training data.

2. Methods

2.1. Data and Models

We assess the ability of the AI model GraphCast to reproduce the global diurnal precipitation cycle during boreal summer by comparing its June–August (JJA) 2023 forecasts with ERA5, the IMERG satellite product, and an experimental global 5-km scale UM configuration from the Met Office.

GraphCast forecasts were generated using the ECMWF AI-models toolbox. GraphCast is a deep learning system trained on about 40 years of ERA5 atmospheric and surface fields (Hersbach et al., 2020) at 0.25° resolution (approximately 30 km). Because it is autoregressive, outputs from each forecast step become inputs to the next. Below we outline the characteristics of GraphCast, IMERG, ERA5, and the UM simulation.

- *GraphCast*: GraphCast employs a Graph Neural Network with roughly 36.7 million parameters. It predicts five surface variables and six pressure-level variables on 37 vertical levels. The encoder projects grid-cell information onto a multiresolution icosahedral mesh (12–40,962 nodes), followed by 16 processor layers that propagate information across scales via message passing. The decoder maps node representations back to a regular latitude-longitude grid, avoiding the scalability limitations often encountered in transformer-based models (Battaglia et al., 2018; Lam et al., 2023). GraphCast outputs 6-hourly accumulated precipitation. We converted these values to instantaneous rates and concatenated daily forecasts initialized at 00:00 UTC to form a continuous JJA 2023 data set. Although precipitation is part of the training data, GraphCast has no architecture specifically optimized for precipitation skill, despite the spatial sparsity and non-Gaussian behavior of rainfall.
- *IMERG*: The IMERG product (Huffman et al., 2015) provides 30-min global precipitation estimates at 0.1° resolution. Its high temporal sampling enables detailed analysis of diurnal amplitude and phase. Limitations include reduced performance near coastlines due to distinct land-ocean retrieval algorithms, underestimation of light rainfall (relevant for nocturnal and maritime precipitation), and larger uncertainties over snow-covered regions, though the latter is less important for JJA.
- *ERA5*: ERA5 (Hersbach et al., 2020) provides hourly global fields at 0.25° resolution and 37 pressure levels. Precipitation is a diagnostic from short-range forecasts within the data assimilation system rather than an

assimilated variable. We use the hourly mean precipitation rate for consistency with IMERG. ERA5 precipitation remains limited by convection parametrization and under-resolved orography.

- *UM 5-km experimental simulation*: We use the Met Office's global 5 km configuration developed for DYAMOND-3 and the Met Office km-scale program. At this resolution, deep convection is largely explicitly represented, improving the simulation of convective organization and the diurnal precipitation cycle relative to coarser models (Tomassini, 2025; Tomassini et al., 2023). The configuration uses a 5 km horizontal grid (N2560), about 85 vertical levels, and the GA9.0 physics suite with a scale-aware, partially resolved convection scheme based on a reduced CoMORPH-A formulation (Lock et al., 2024). The simulation consists of 15-day forecasts initialized every 3 days and coupled to a 10-km ocean model. A continuous JJA 2021 data set was constructed by concatenating the first 3 days of each forecast. Because GraphCast was trained on ERA5 data through 2021, the UM JJA 2021 period cannot be used for direct evaluation of the AI system. We therefore analyze UM JJA 2021 as a reference for 5-km model behavior, and GraphCast JJA 2023 as an independent test period.

2.2. Computing the Diurnal Precipitation Cycle

All data sets were regridded to the ERA5 0.25° grid and sampled at 6-hr intervals. Although IMERG, ERA5, and the UM provide hourly data, GraphCast offers only 6-hourly precipitation, which motivates adopting a common 6-hr temporal sampling across all data sets analyzed in this study. At each grid point, we applied a discrete Fourier transform to extract the dominant diurnal harmonic following Zhang et al. (2024):

$$F(t') = F_0 + S_1(t') + \text{residual}, \qquad S_n(t') = A_n \sin(nt' + \sigma_n),$$

where F_0 is the mean precipitation rate, and A_n and σ_n are the amplitude and phase of the nth harmonic. Local solar time (LST) at longitude λ is defined as

$$\text{LST} = \text{UTC} + \lambda/15° \text{ hours},$$

where 15° corresponds to 1 hour of Earth's rotation. The first harmonic S_1 provides the diurnal amplitude (A_1) and the local time of maximum precipitation (σ_1). Although higher harmonics such as the semi-diurnal component can contribute locally, the first harmonic captures most of the global variance in precipitation timing and intensity (Dai, 2001; Curt et al., 2016; S. Yang & Smith, 2006).

3. Results

3.1. IMERG Global Diurnal Precipitation Cycle in Boreal Summer

Figure 1 shows IMERG JJA mean precipitation, amplitude, and phase over the Central U.S. Great Plains for 2021 and 2023, included to verify that interannual variability does not affect comparisons with GraphCast and the UM 5-km model simulation.

Figures 1a and 1b indicate that the spatial distribution of mean precipitation is highly consistent across the JJA2021 and JJA2023, with intense rainfall along the Intertropical Convergence Zone (ITCZ) and major monsoon regions. JJA 2023 is slightly wetter over the western Pacific and tropical Atlantic (≈ 2 mm day^{-1}), while 2021 shows modestly drier conditions over some subtropical land areas.

The diurnal amplitude and phase fields (Figures 1c–1f) also show minimal interannual differences. Amplitude peaks over continental interiors and coastal regions where land-sea-breeze circulations promote convection, reaching 3–7 mm day^{-1}. Large values occur over central Africa, the Maritime Continent, and the western Pacific warm pool, while open oceans and extratropical latitudes show weak diurnal modulation dominated by synoptic variability.

IMERG phase patterns in both years confirm a robust late-afternoon to early evening precipitation maximum over land (≈15–19 LST) and an early morning maximum (≈03–06 LST) over tropical oceans. Several coastal regions (e.g., Gulf of Mexico, Central America, South and Southeast Asia) exhibit a secondary near-midday peak linked to sea-breeze interactions. Patchiness over the Southern Ocean reflects migrating midlatitude storm systems.

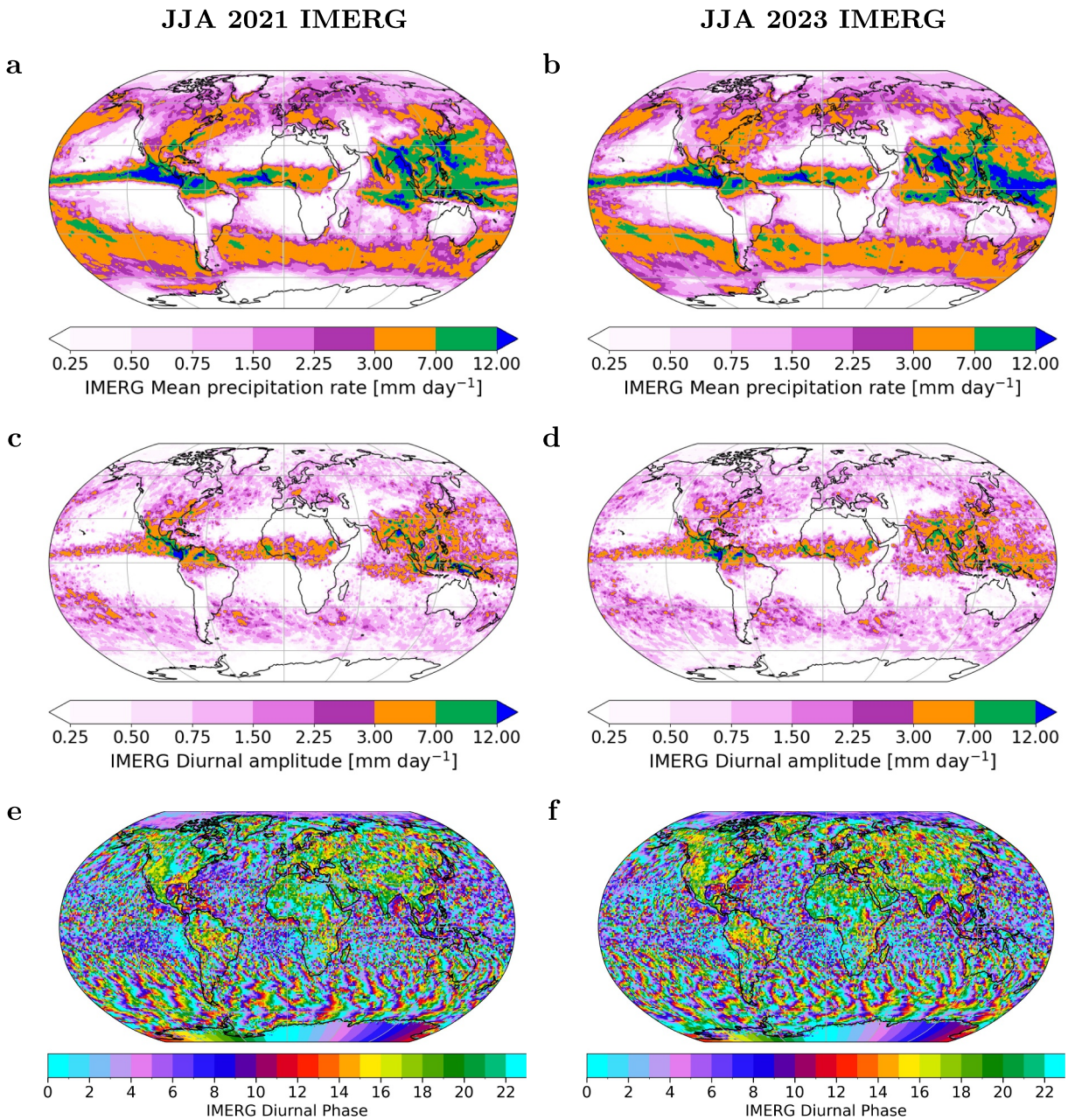

Figure 1. Global mean precipitation characteristics and diurnal cycle during boreal summer JJA. Panels (a, c, and e) show the (a) mean precipitation rate (mm day^{-1}), (c) amplitude (mm day^{-1}), and (e) phase (hour of maximum in Local solar time [LST]) derived from the Integrated Multi-satellite Retrievals for GPM observational product for the 2021 JJA. Panels (b, d, and f) display the corresponding fields from the 2023 JJA. Phase is defined as the LST peak precipitation in the diurnal harmonic, and amplitude corresponds to the magnitude of the first harmonic. The phase scale is circular (0–24 LST), with warmer colors indicating afternoon peak times, while cooler colors indicating night or early morning peak times.

Mountainous regions show slightly earlier afternoon peaks, while arid and subtropical regions display weak or intermittent diurnal signals.

The similarity between IMERG 2021 and 2023 indicates weak interannual variability in the diurnal cycle, supporting the use of the UM 5-km simulation from JJA 2021 for comparison with GraphCast and ERA5.

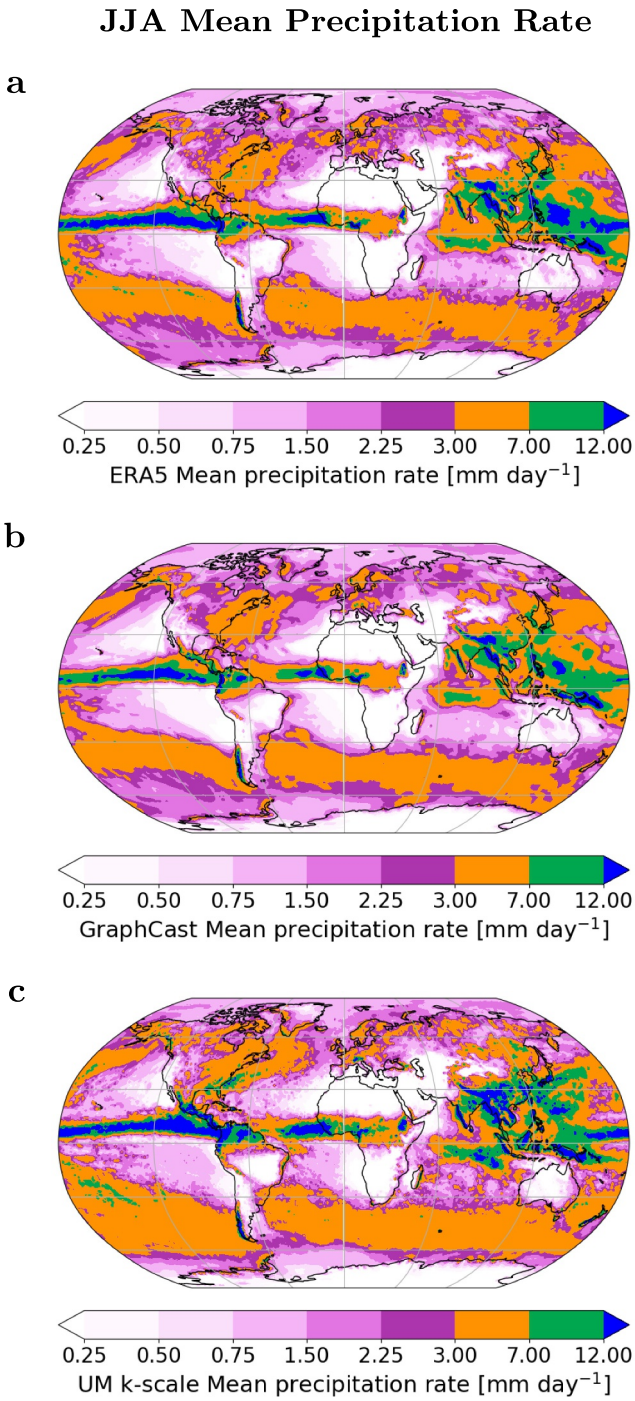

Figure 2. Mean precipitation rate as in Figures 1a and 1b but for (a) ERA5, (b) GraphCast, and the (c) Unified Model (UM) 5-km model. Note that ERA5 and GraphCast refer to JJA 2021 while the UM 5-km simulation to JJA 2023.

3.2. ERA5, GraphCast, and UM 5-km Experimental Model Capability in Capturing Mean Precipitation Rate, Amplitude, and Phase

The ERA5 reanalysis well reproduces the global structure of the IMERG mean precipitation rate (Figure 2a). It captures the main precipitation maxima exceeding 12 mm day^{-1} along the ITCZ and over the Maritime Continent, as well as secondary maxima of 3–7 mm day^{-1} across regions such as the Great Plains, central Africa, and the Southern Ocean. However, ERA5 overestimates mean precipitation by approximately 2 mm day^{-1} along the eastern Pacific ITCZ and underestimates it by a similar magnitude across extensive areas of the Maritime Continent.

GraphCast broadly reproduces the ERA5 spatial distribution of mean precipitation rate (Figure 2b), including the location of the primary mean rate precipitation maxima, with rates occasionally exceeding 12 mm day^{-1} along the ITCZ and over the Maritime Continent. Moreover, the spatial distribution of mean precipitation rate predicted by GraphCast over North America and the Southern Ocean is broadly consistent with ERA5 and IMERG. However, the regions of maximum mean precipitation are considerably smaller in GraphCast than in ERA5, with underestimations up to $\approx$ 5 mm day^{-1} across parts of the Atlantic and Pacific ITCZ and around Mexico.

The experimental UM 5-km model simulation (Figure 2c) reproduces the spatial distribution of the IMERG mean precipitation rate more accurately, particularly in capturing the location and magnitude of tropical rainfall maxima. However, it substantially overestimates precipitation in the mid-latitudes, most notably over the Southern Ocean but also across Europe and central to eastern North America, a bias that neither GraphCast nor ERA5 exhibited. In the Southern Ocean, areas with mean precipitation of 5–7 mm day^{-1} cover nearly twice the extent indicated by IMERG, suggesting excessive frontal precipitation in this region.

When considering the diurnal amplitude of ERA5 precipitation (Figure 3a), larger discrepancies relative to IMERG arise than for the mean precipitation rate. More in details, ERA5 exhibits a less organized and more fragmented amplitude structure, particularly over the Great Plains, where the amplitude rarely exceeds 1.5–2 mm day^{-1}, and over the Maritime Continent, where, although values reach up to 7–10 mm day^{-1}, the areas of strong diurnal variability are considerably smaller and more spatially discontinuous than in IMERG. Around the coastal regions of Mexico, the amplitude barely reaches 7–10 mm day^{-1}, while in IMERG they exceed 12 mm day^{-1}.

Graphcast appears to inherit and amplify ERA5 underestimations in the precipitation amplitude of the first diurnal harmonic, with Figure 3b showing the amplitude systematically weaker, by up to 3 mm day^{-1}, over both primary and secondary convective regions, including the Maritime Continent, ITCZ, and the Great Plains. Central Africa exhibits a similar negative bias, while amplitudes over the Southern Ocean and North Atlantic remain smaller than in both ERA5 and IMERG.

The diurnal amplitude in the UM 5-km simulation (Figure 3c) closely matches IMERG across most regions, with only minor differences: a slight underestimate of up to ~1 mm day^{-1} over the Great Plains and a modest overestimate of ~1.5 mm day^{-1} over the Maritime Continent. Elsewhere, such as central Africa, the Gulf of Mexico, the ITCZ, and the midlatitude oceans, the amplitude agrees well with IMERG.

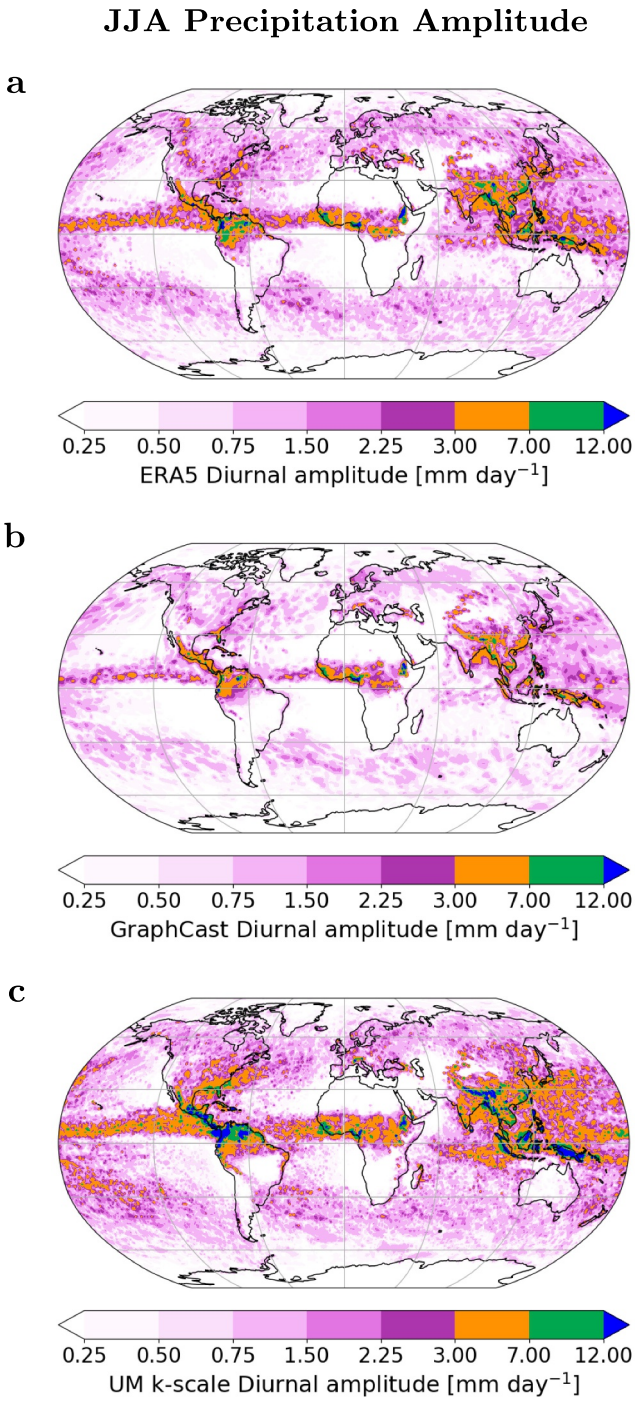

Figure 3. Diurnal amplitude of precipitation as in Figures 1c and 1d but for (a) ERA5, (b) GraphCast, and the (c) Unified Model 5-km model.

Finally, we analyze the precipitation phase (precipitation peak timing) in Figure 4. The ERA5 precipitation peak timing displays substantial biases (Figure 4a), especially over land. Over the Amazon, central Africa, continental Europe, the United States, and Siberia, the diurnal maximum is shifted toward midday or early afternoon (approximately 12–16 LST), rather than the late-afternoon to evening peak observed in IMERG. This premature peak is a well-known feature of ERA5 and arises from the convective parameterization in the IFS model, which tends to trigger convection too early in the day in response to rapid surface heating and boundary-layer growth, before sufficient moistening and instability have developed to support deep convection as observed in IMERG. In contrast, regions dominated by frontal-driven precipitation, such as the Southern Ocean, show similar patchy phase structures to those in IMERG.

The timing of the diurnal precipitation maximum (phase) in GraphCast also shows systematic biases (Figure 4b). Over land, precipitation peaks nearly everywhere between late morning and early afternoon (approximately 11:00–14:00 LST), amplifying the premature convective onset already present in ERA5 and further degrading its midday bias. Exceptions include the Great Plains, southern South America, and southern Africa, where the phase aligns more closely with observations. Over oceans, GraphCast precipitation peaks too early, typically between 1 and 3 LST, whereas both ERA5 and IMERG indicate a later maximum between 7 and 10 LST. Frontal precipitation regions over the North Atlantic and Southern Ocean display similar patchy phase structures to ERA5, reflecting the model's inherited large-scale dynamics rather than localized convective processes.

While the experimental UM 5-km model improved the precipitation diurnal amplitude relative to IMERG compared to ERA5, the timing of the diurnal precipitation maximum (phase) exhibits larger regional biases, in particular over land (Figure 4c). Notably, spurious midday peaks occur across parts of central and southern Africa as well as across the western and central United States. Similarly (and again relatively degraded) to ERA5, continental regions such as Siberia and Europe also display an unrealistically synchronized midday maximum, indicative of an overly rapid convective response to surface heating. However, there are some notable exceptions, that is regions where the experimental UM 5-km model does well capture the diurnal precipitation phase. For instance, the model realistically simulates a midday peak over South America, albeit occurring a few hours earlier than the early afternoon maximum observed in IMERG. It also reproduces the early morning and spatially patchy phase structure over the Maritime Continent, as well as the characteristic frontal-driven "comma-shaped" phase alternations over the Southern Ocean.

We repeated the diurnal diagnostics using five JJA seasons (2021–2025) for GraphCast, IMERG, and ERA5 (Figures S1–S6 in Supporting Information S1) to assess sensitivity to multi-year sampling. While averaging modestly improves spatial coherence where the diurnal signal is strong, it does not materially change phase structure, amplitude, or model-observation differences. Because km-scale output is unavailable only for extended multi-years JJA seasons, we retain same-season comparisons to ensure consistent temporal sampling. This highlights the need for longer km-scale integrations to enable systematic skill assessment of key fields such as precipitation, which lies beyond the scope of this study.

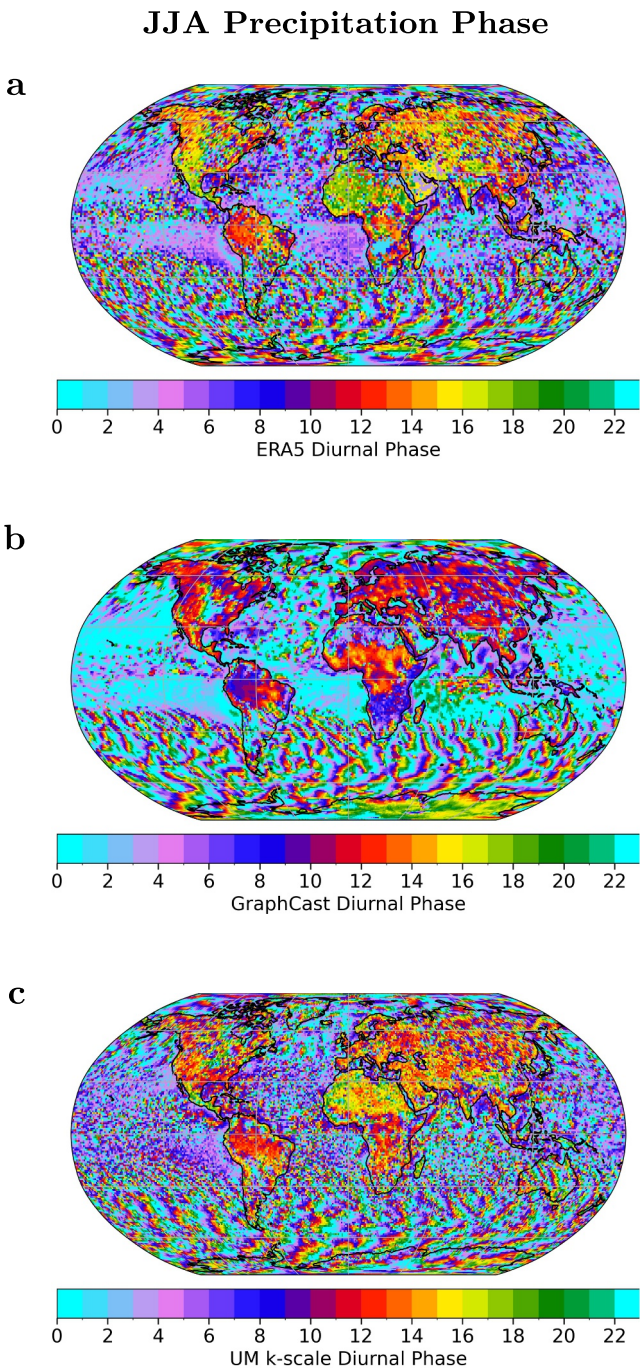

Figure 4. Phase of precipitation as in Figures 1e and 1f but for (a) ERA5, (b) GraphCast, and the (c) Unified Model 5-km experimental model.

3.3. Land-Ocean Contrast in IMERG, ERA5, GraphCast, and the UM 5-km Experimental Model

To better examine regional contrasts and quantify land-ocean differences in model performance, we show and compare in Figure 5 domain-averaged diurnal precipitation without projection onto a single harmonic for IMERG JJA 2021 and 2023, ERA5 (2023), GraphCast (2023), and the UM 5-km model (2021).

The two IMERG seasons exhibit only minor differences, less than 0.25 mm day^{-1} across all regions, with 2023 showing slightly higher totals, consistent with Figure 1. This further confirms that the seasonal mismatch between the UM 5-km simulation (2021) and ERA5/GraphCast (2023) data sets does not compromise intercomparison, as already discussed in Figure 1.

ERA5 broadly reproduces the tropical-ocean diurnal cycle but exhibits pronounced biases over land (±50° latitude). Precipitation peaks too early in the afternoon and is markedly underestimated at night. Regionally, ERA5's diurnal maximum occurs ≈2 hr earlier than IMERG over Africa and Asia, while Europe and the central United States display a more realistic late-afternoon peak. Nighttime rainfall is systematically too weak, with deficits of ≈2 mm day^{-1} over Asia and the central U.S., ≈1 mm day^{-1} over Africa, and ≈0.5 mm day^{-1} over Europe relative to IMERG (Figure 5a).

The UM 5-km simulation exhibits a substantially stronger diurnal amplitude than IMERG and ERA5, with peak precipitation occurring ≈3 hr earlier than IMERG and earlier than ERA5 in several regions. Thus, in terms of amplitude and phase, it does not represent an overall improvement over ERA5. However, it produces enhanced nocturnal precipitation over global land, including Africa and the central United States, partially reducing ERA5's nighttime deficit. While this likely reflects explicitly resolved convective organization at kilometer scale, convection remains triggered too readily, contributing to the premature afternoon maximum. ERA5 precipitation is also indirectly constrained by data assimilation, whereas the UM 5-km simulation is a free-running forecast re-initialized every 72 hr, the two are therefore not directly comparable in overall skill.

GraphCast shows a comparable or larger phase bias, with precipitation peaking ≈4 hr earlier than IMERG over global land (Figure 5a) and exhibiting a pronounced nighttime deficit. The phase centers in late morning to early afternoon, consistent with the 10–14 LST peak identified in Figure 4c, leading to rainfall being concentrated near local noon. Although the present analysis does not directly diagnose convective organization, this bias suggests an overrepresentation of daytime processes and underrepresentation of nocturnal rainfall. A caveat is the native 6-hourly GraphCast output: while hourly curves are derived after LST conversion and interpolation, the limited temporal sampling reduces the number of independent time points entering the harmonic analysis. This may affect quantitative precision but does not alter the qualitative early peaking structure.

4. Discussion and Conclusions

This study provides a process-based evaluation of the ability of the AI weather prediction model GraphCast to reproduce the global diurnal cycle of summertime (JJA) precipitation, relative to IMERG, ERA5, and an experimental global 5-km convection-permitting configuration of the Met Office UM. Although leading AI systems such as GraphCast approach or exceed NWP skill for smooth synoptic fields at far lower computational

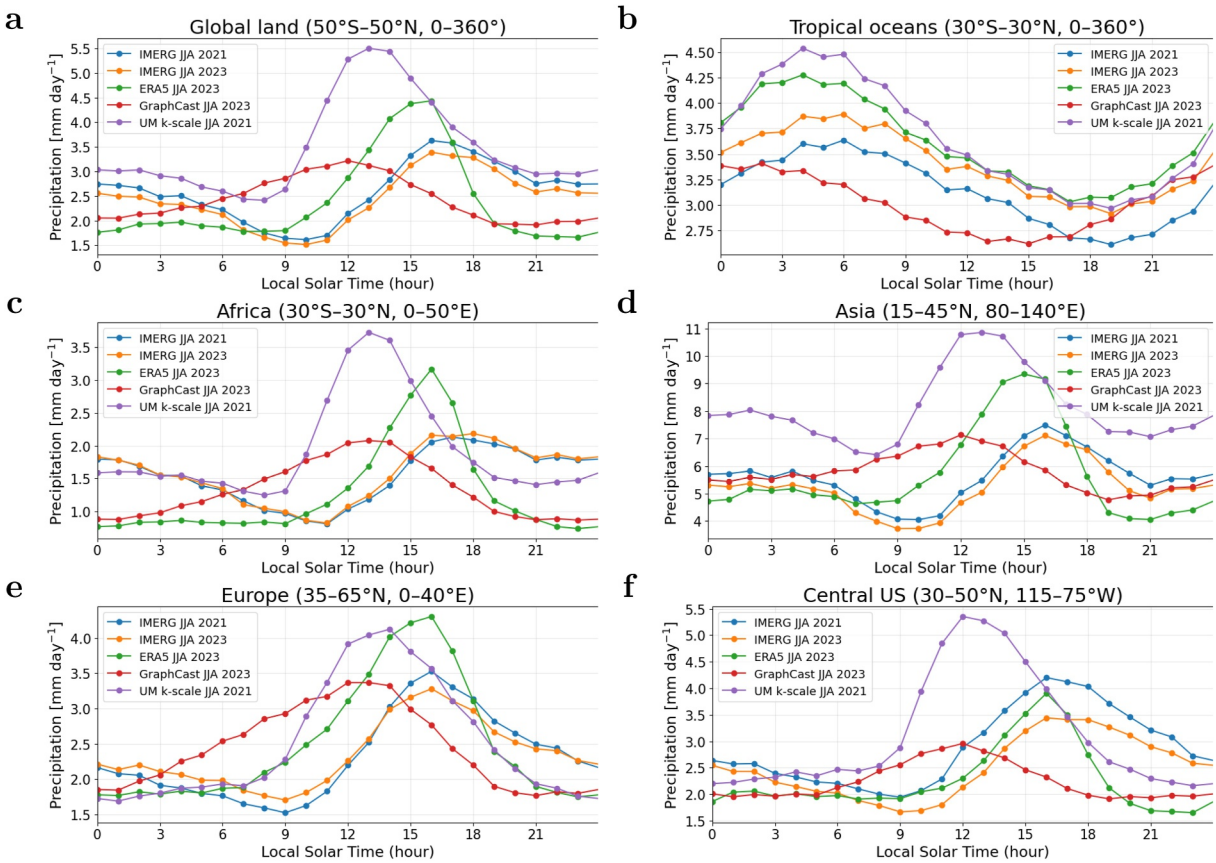

Figure 5. Domain averaged hourly precipitation (units: mm day^{-1}) without projection to first harmonic over (a) global land, (b) tropical ocean, (c) Africa (d) Asia, (e) Europe, and (f) Central US for Integrated Multi-satellite Retrievals for GPM (IMERG) JJA2021 (blue lines), IMERG JJA 2023 (orange lines), ERA5 JJA 2023 (green lines), GraphCast JJA 2023 (red lines), and Unified Model 5-km JJA 2021 (purple lines).

cost (e.g., 500 hPa geopotential height), their representation of higher-order physical variability, including the diurnal cycle, remains insufficiently understood.

Analysis of mean rate, amplitude, and phase shows that GraphCast inherits ERA5 strengths and weaknesses, and often amplifies the latter. It captures the spatial distribution of mean rainfall, including 12 mm day^{-1} maxima along the ITCZ and Maritime Continent, but underestimates diurnal amplitude by up to 5 mm day^{-1} relative to IMERG and performs worse than ERA5 in this metric, consistent with known ERA5 limitations (Dai, 2024; Pradhan et al., 2025; Watters et al., 2021) and similar issues in MERRA-2 (Reichle et al., 2017).

GraphCast also worsens the timing of the diurnal cycle, placing peak land rainfall in late morning to early afternoon, about 4 hr early relative to IMERG and 2 hr early relative to ERA5, mirroring premature triggering in the IFS used for ERA5 (Bechtold et al., 2014). In addition, GraphCast shows substantially reduced nocturnal precipitation in regions where observations exhibit pronounced nighttime maxima, including parts of Africa, Asia, and the central United States, indicating a systematic nighttime deficit relative to IMERG (and the 5-km UM). Although the present diagnostics do not directly resolve mesoscale organization or cold-pool dynamics that govern nocturnal rainfall, the combination of an early daytime peak and suppressed nighttime precipitation is consistent with an overrepresentation of locally timed daytime processes.

These compressed amplitudes and early phases align with broader evidence of physical limitations in current ML weather models (Bonavita, 2024). Weak nocturnal rainfall likely reflects both missing mesoscale organization and under-resolved contributions from large-scale processes such as nocturnal low-level jets and circulation-driven moisture convergence (Liang & Zhang, 2021; Ma et al., 2024; Ousmane et al., 2024). Since ERA5 precipitation is not directly assimilated and contains systematic timing biases, GraphCast likely learns from biased labels. Its coarse (0.25°, 6-hourly) resolution constrains mesoscale convective system propagation, while losses

on sparse, heavy-tailed rainfall fields tend to smooth amplitudes (Hunt, 2025; Lam et al., 2023). Autoregressive drift may further worsen timing errors in CAPE, CIN, and moisture convergence.

In contrast, the global UM 5-km experimental simulation improves both amplitude and nocturnal phase over land and ocean, particularly across the central United States, Africa, and the Maritime Continent. These improvements stem from resolving deep convection and mesoscale processes largely absent or heavily parameterized in coarser models (Tomassini et al., 2023). More realistic convective organization enhances nighttime precipitation and brings the UM closer to IMERG. However, the UM retains a substantial wet bias (Takasuka et al., 2025; Tomassini, 2025), likely linked to sensitivities in microphysics and boundary-layer and air-sea coupling. It also produces an afternoon peak 3 hr early, potentially arising from the scale-aware convective parametrization (Lavender et al., 2024; Lock et al., 2024), which remains active at 5 km and may trigger convection ahead of the observed onset under daytime heating.

Overall, neither GraphCast nor the experimental 5-km UM fully resolves longstanding biases in the diurnal precipitation cycle. Because accurately capturing the diurnal cycle relies on processes spanning convective initiation, turbulence-microphysics coupling, and surface-atmosphere feedbacks (Pearson et al., 2014), persistent errors across model paradigms indicate that progress must focus on improving sub-grid physical process representation, whether in conventional or AI-based models. The diurnal cycle thus remains a valuable, physically interpretable benchmark that should be routinely incorporated into future model development and evaluation.

Future work should prioritize improving physical-process closures in km-scale models, including turbulence, convection, and microphysics (Bogenschutz & Krueger, 2013; De Roode et al., 2019; Gentile et al., 2025; Honnert et al., 2020; Larson et al., 2019; Nardi et al., 2024), while advancing AI systems toward learning the governing dynamics of moist convection rather than replication of statistical patterns (Bonavita, 2024; Hunt, 2025; Lam et al., 2023; Pathak et al., 2022; Selz & Craig, 2023). A complementary strategy emerging at operational centers applies scale-selective spectral nudging, constraining large-scale modes ($\approx 1000-2000$ km and above) of a physical model toward an AI forecast while allowing smaller scales to evolve freely (Husain et al., 2025). Hybrid AI-physics frameworks, combining the physical realism of km-scale simulations with the computational efficiency of AI (Das et al., 2024; Driscoll et al., 2025; Schneider et al., 2023; Shamekh & Gentine, 2023; Slater et al., 2023; Wang et al., 2025) offer a promising route for improving precipitation timing, amplitude, and spatial variability across scales.

Conflict of Interest

The authors declare no conflicts of interest relevant to this study.

Availability Statement

The ERA5 data are available at Hersbach et al. (2023). IMERG data sets are from Huffman et al. (2023). Model data and analysis code that support the findings of this study are available at Gentile (2026a, 2026b).

Acknowledgments
We thank Michael Whitall, Sally Lavender, and Tim Graham for their contributions to the kilometer-scale Met Office Unified Model and its coupled configuration. ESG, BJH, and OMA were partly funded by the NERC CANARI project (NE/W004984/1) during this work.

References

Arai, R., Sato, T., & Imamura, M. (2025). Evaluating the precipitation prediction skill by GraphCast in the Japan region. *Transactions of the Japan Society of Civil Engineers*, *81*(16), 24–16106. https://doi.org/10.2208/jscejj.24-16106

Battaglia, P. W., Hamrick, J. B., Bapst, V., Sanchez-Gonzalez, A., Zambaldi, V., Malinowski, M., et al. (2018). Relational inductive biases, deep learning, and graph networks. *arXiv preprint arXiv:1806.01261*. https://doi.org/10.48550/arXiv.1806.01261

Bechtold, P., Chaboureau, J.-P., Beljaars, A., Betts, A. K., Köhler, M., Miller, M., & Redelsperger, J.-L. (2004). The simulation of the diurnal cycle of convective precipitation over land in a global model. *Quarterly Journal of the Royal Meteorological Society*, *130*(604), 3119–3137. https://doi.org/10.1256/qj.03.103

Bechtold, P., Semane, N., Lopez, P., Chaboureau, J.-P., Beljaars, A., & Bormann, N. (2014). Representing equilibrium and nonequilibrium convection in large-scale models. *Journal of the Atmospheric Sciences*, *71*(2), 734–753. https://doi.org/10.1175/jas-d-13-0163.1

Berthou, S., Rowell, D. P., Kendon, E. J., Roberts, M. J., Stratton, R. A., Crook, J. A., & Wilcox, C. (2019). Improved climatological precipitation characteristics over West Africa at convection-permitting scales. *Climate Dynamics*, *53*(3–4), 1991–2011. https://doi.org/10.1007/s00382-019-04759-4

Bogenschutz, P. A., & Krueger, S. K. (2013). A simplified PDF parameterization of subgrid-scale clouds and turbulence for cloud-resolving models. *Journal of Advances in Modeling Earth Systems*, *5*(2), 195–211. https://doi.org/10.1002/jame.20018

Bonavita, M. (2024). On some limitations of current machine learning weather prediction models. *Geophysical Research Letters*, *51*(12), e2023GL107377. https://doi.org/10.1029/2023gl107377

Christopoulos, C., & Schneider, T. (2021). Assessing biases and climate implications of the diurnal precipitation cycle in climate models. *Geophysical Research Letters*, *48*(13), e2021GL093017. https://doi.org/10.1029/2021gl093017

Curt, C., Peter, J. G., Kenneth, R. S., & Santer, B. M. (2016). Metrics for the diurnal cycle of precipitation: Toward routine benchmarks for climate models. *Journal of Climate*, *29*, 4461–4471. https://doi.org/10.1175/JCLI-D-15-0664.1

Dai, A. (2001). Global precipitation and thunderstorm frequencies. Part II: Diurnal variations. *Journal of Climate*, *14*(6), 1112–1128. https://doi.org/10.1175/1520-0442(2001)014<1112:gpatfp>2.0.co;2

Dai, A. (2006). Precipitation characteristics in eighteen coupled climate models. *Journal of Climate*, *19*(18), 4605–4630. https://doi.org/10.1175/jcli3884.1

Dai, A. (2024). The diurnal cycle from observations and ERA5 in precipitation, clouds, boundary layer height, buoyancy, and surface fluxes. *Climate Dynamics*, *62*, 5879–5908. https://doi.org/10.1007/s00382-024-07182-6

Dai, A., & Trenberth, K. E. (2004). The diurnal cycle and its depiction in the community climate system model. *Journal of Climate*, *17*(5), 930–951. https://doi.org/10.1175/1520-0442(2004)017<0930:tdcaid>2.0.co;2

Das, P., Posch, A., Barber, N., Hicks, M., Duffy, K., Vandal, T., et al. (2024). Hybrid physics-AI outperforms numerical weather prediction for extreme precipitation nowcasting. *npj Climate and Atmospheric Science*, *7*(1), 282. https://doi.org/10.1038/s41612-024-00834-8

De Roode, S., Frederikse, T., Siebesma, A., Ackerman, A., Chylik, J., Field, P., et al. (2019). Turbulent transport in the gray zone: A large eddy model intercomparison study of the CONSTRAIN cold air outbreak case. *Journal of Advances in Modeling Earth Systems*, *11*(3), e2018MS001443. https://doi.org/10.1029/2018ms001443

Driscoll, S., Hunt, K. M. R., Mansfield, L., Swaminathan, R., Wei, H., Bach, E., et al. (2025). *Weather and climate: Applications of machine learning and artificial intelligence*. Elsevier.

Edwards, J., Beljaars, A., Holtslag, A., & Lock, A. P. (2020). Representation of boundary-layer processes in numerical weather prediction and climate models. *Boundary-Layer Meteorology*, *177*(2–3), 511–539. https://doi.org/10.1007/s10546-020-00530-z

Fang, J., & Du, Y. (2022). A global survey of diurnal offshore propagation of rainfall. *Nature Communications*, *13*, 7437. https://doi.org/10.1038/s41467-022-34842-0

Feng, Z., Leung, L. R., Hardin, J., Terai, C. R., Song, F., & Caldwell, P. (2023). Mesoscale convective systems in Dyamond global convection-permitting simulations. *Geophysical Research Letters*, *50*(4), e2022GL102603. https://doi.org/10.1029/2022gl102603

Gentile, E. S. (2026a). Dataset of hourly averaged precipitation cycle [Dataset]. https://doi.org/10.5281/zenodo.18760623

Gentile, E. S. (2026b). Python code for precipitation diurnal cycle [Software]. https://doi.org/10.5281/zenodo.18760541

Gentile, E. S., Larson, V. E., Zhao, M., Zarzycki, C. M., Svensson, G., & Donner, L. (2025). Enhancing great plains nocturnal precipitation and low-level jets in AM4 with an extended CLUBB closure. *Authorea Preprint*. https://doi.org/10.22541/au.175519398.83690415/v1

Harris, L., Zhou, L., Lin, S., Chen, J., Chen, X., Gao, K., et al. (2020). GFDL SHiELD: A unified system for weather-to-seasonal prediction. *Journal of Advances in Modeling Earth Systems*, *12*(10), e2020MS002223. https://doi.org/10.1029/2020ms002223

Hersbach, H., Bell, B., Berrisford, P., Biavati, G., Horányi, A., Muñoz Sabater, J., et al. (2023). ERA5 hourly data on single levels from 1940 to present [Dataset]. *Copernicus Climate Change Service (C3S) Climate Data Store (CDS)*. https://doi.org/10.24381/cds.adbb2d47

Hersbach, H., Bell, B., Berrisford, P., Hirahara, S., Horányi, A., Muñoz-Sabater, J., et al. (2020). The ERA5 global reanalysis. *Quarterly Journal of the Royal Meteorological Society*, *146*(730), 1999–2049. https://doi.org/10.1002/qj.3803

Honnert, R., Efstathiou, G. A., Beare, R. J., Ito, J., Lock, A., Neggers, R., et al. (2020). The atmospheric boundary layer and the "gray zone" of turbulence: A critical review. *Journal of Geophysical Research: Atmospheres*, *125*(13), e2019JD030317. https://doi.org/10.1029/2019jd030317

Hu, H., Leung, L. R., & Feng, Z. (2021). Early warm-season mesoscale convective systems and soil moisture–precipitation feedbacks in the central United States. *Proceedings of the National Academy of Sciences of the United States of America*, *118*, e2109372118. https://doi.org/10.1073/pnas.2105260118

Huffman, G. J., Bolvin, D. T., Braithwaite, D., Hsu, K., Joyce, R., Kidd, C., et al. (2015). *NASA global precipitation measurement (GPM) integrated multi-satellite retrievals for GPM (IMERG) (algorithm theoretical basis document no. Version 4.5)* (p. 26). NASA.

Huffman, G. J., Stocker, E. F., Bolvin, D. T., Nelkin, E. J., & Tan, J. (2023). GPM IMERG final precipitation L3 half hourly 0.1 degree x 0.1 degree V07 [Dataset]. *Goddard Earth Sciences Data and Information Services Center (GES DISC)*. https://doi.org/10.5067/GPM/IMERG/3B-HH/07

Hunt, K. M. R. (2025). Stop using root-mean-square error as a precipitation target!. *arXiv preprint arXiv:2509.08369*. https://doi.org/10.48550/arXiv.2509.08369

Husain, S. Z., Separovic, L., Caron, J.-F., Aider, R., Buehner, M., Chamberland, S., et al. (2025). Leveraging data-driven weather models for improving numerical weather prediction skill through large-scale spectral nudging. *Weather and Forecasting*, *40*(9), 1749–1771. https://doi.org/10.1175/WAF-D-24-0139.1

Jensen, G. G., Fiévet, R., & Haerter, J. O. (2022). The diurnal path to persistent convective self-aggregation. *Journal of Advances in Modeling Earth Systems*, *14*(5), e2021MS002953. https://doi.org/10.1029/2021ms002923

Jones, R. W., Sanchez, C., Lewis, H., Warner, J., Webster, S., & Macholl, J. (2023). Impact of domain size on tropical precipitation within explicit convection simulations. *Geophysical Research Letters*, *50*(17), e2023GL104672. https://doi.org/10.1029/2023gl104672

Lam, R., Pathak, J., Subramanian, S., Kashinath, K., Kurth, T., Hall, D., et al. (2023). Learning skillful medium-range global weather forecasting. *Science*, *382*(6677), 1416–1421. https://doi.org/10.1126/science.adi2336

Larson, V., Domke, S., & Griffin, B. M. (2019). Momentum transport in shallow cumulus clouds and its parameterization by higher-order closure. *Journal of Advances in Modeling Earth Systems*, *11*, 3419–3442. https://doi.org/10.1029/2019ms001743

Lavender, S. L., Stirling, A. J., Whitall, M., Stratton, R. A., Daleu, C. L., Plant, R. S., et al. (2024). The use of idealised experiments in testing a new convective parametrization: Performance of CoMorph-A. *Quarterly Journal of the Royal Meteorological Society*, *150*(760), 1581–1600. https://doi.org/10.1002/qj.4660

Liang, X., & Zhang, M. (2021). Summer and winter precipitation in east Asia scale with global warming at different rates. *Communications Earth & Environment*, *2*(1), 150. https://doi.org/10.1038/s43247-021-00219-2

Lock, A. P., Whitall, M., Stirling, A. J., Williams, K. D., Lavender, S. L., Morcrette, C., et al. (2024). The performance of the CoMorph-A convection package in global simulations with the Met Office Unified model. *Quarterly Journal of the Royal Meteorological Society*, *150*(763), 3527–3543. https://doi.org/10.1002/qj.4781

Ma, X., Li, Y., Li, Z., & Huo, F. (2024). Investigation of the characteristics of low-level jets over North America in a convection-permitting weather research and forecasting simulation. *Atmospheric Chemistry and Physics*, *24*(20), 12013–12030. https://doi.org/10.5194/acp-24-12013-2024

Nardi, K., Zarzycki, C., Larson, V., & Bryan, G. (2024). A method for interpreting the role of parameterized turbulence on global metrics in the community Earth system model. *Journal of Advances in Modeling Earth Systems*, *16*(10), e2024MS004482. https://doi.org/10.1029/2024ms004482

Nesbitt, S. W., & Zipser, E. J. (2003). The diurnal cycle of rainfall and convective intensity according to three years of TRMM measurements. *Journal of Climate*, *16*(10), 1456–1475. https://doi.org/10.1175/1520-0442-16.10.1456

O'Gorman, P. A., Li, Z., Boos, W. R., & Yuval, J. (2021). Response of extreme precipitation to uniform surface warming in quasi-global aquaplanet simulations at high resolution. *Philosophical Transactions of the Royal Society A: Mathematical, Physical and Engineering Sciences*, *379*(2195), 20190543. https://doi.org/10.1098/rsta.2019.0543

Ousmane, M. R. I., Abdou Saley, I., Abdoul Aziz, S. C., Moussa, M. S., Diakaria, K., Sanda, I. S., et al. (2024). Could ERA5 deliver better climate services than ERA-interim over the West African Sahel Region? *Journal of Environmental Engineering and Science*, *13*, 144–158.

Pathak, J., Subramanian, S., Harrington, P., Raja, S., Chattopadhyay, A., Mardani, M., et al. (2022). Fourcastnet: A global data-driven high-resolution weather model using adaptive Fourier neural operators. *arXiv preprint arXiv:2202.11214*. https://doi.org/10.48550/arXiv.2202.11214

Pearson, K. J., Lister, G. M. S., Birch, C. E., Allan, R. P., Hogan, R. J., & Woolnough, S. J. (2014). Modelling the diurnal cycle of tropical convection across the "grey zone". *Quarterly Journal of the Royal Meteorological Society*, *140*(679), 491–499. https://doi.org/10.1002/qj.2145

Pradhan, R. K., Markonis, Y., Marra, F., Nikolopoulos, E. I., Papalexiou, S. M., & Levizzani, V. (2025). Diurnal variability of global precipitation: Insights from hourly satellite and reanalysis datasets. *Hydrology and Earth System Sciences*, *29*(19), 4929–4949. https://doi.org/10.5194/hess-29-4929-2025

Rackow, T., Pedruzo-Bagazgoitia, X., Becker, T., Milinski, S., Sandu, I., Aguridan, R., et al. (2025). Multi-year simulations at kilometre scale with the integrated forecasting system coupled to FESOM2.5 and NEMOv3.4. *Geoscientific Model Development*, *18*(1), 33–69. https://doi.org/10.5194/gmd-18-33-2025

Randall, D. A., Harshvardhan, & Dazlich, D. A. (1991). Diurnal variability of the hydrologic cycle in a general circulation model. *Journal of the Atmospheric Sciences*, *48*(1), 40–62. https://doi.org/10.1175/1520-0469(1991)048<0040:dvothc>2.0.co;2

Reichle, R. H., Liu, Q., Koster, R. D., Draper, C. S., Mahanama, S. P. P., & Partyka, G. S. (2017). Land surface precipitation in MERRA-2. *Journal of Climate*, *30*(5), 1643–1664. https://doi.org/10.1175/jcli-d-16-0570.1

Satoh, M., Stevens, B., Judt, F., Khairoutdinov, M., Lin, S.-J., Putman, W. M., & Düben, P. (2019). Global cloud-resolving models. *Current Climate Change Reports*, *5*(3), 172–184. https://doi.org/10.1007/s40641-019-00131-0

Schär, C., Fuhrer, O., Arteaga, A., Ban, N., Charpilloz, C., Di Girolamo, S., et al. (2020). Kilometer-scale climate models: Prospects and challenges. *Bulletin America Meteorology Social*, *101*(5), E567–E587. https://doi.org/10.1175/bams-d-18-0167.1

Schneider, T., Behera, S., Boccaletti, G., Deser, C., Emanuel, K., Ferrari, R., et al. (2023). Harnessing AI and computing to advance climate modelling and prediction. *Nature Climate Change*, *13*(9), 887–889. https://doi.org/10.1038/s41558-023-01769-3

Selz, T., & Craig, G. C. (2023). Can artificial intelligence-based weather prediction models simulate the butterfly effect? *Geophysical Research Letters*, *50*(20), e2023GL105747. https://doi.org/10.1029/2023gl105747

Shamekh, S., & Gentine, P. (2023). Learning atmospheric boundary layer turbulence. *ESS Open Archive*. https://doi.org/10.22541/essoar.168748456.60017486/v1

Slater, L. J., Arnal, L., Boucher, M.-A., Chang, A. Y.-Y., Moulds, S., Murphy, C., et al. (2023). Hybrid forecasting: Blending climate predictions with AI models. *Hydrology and Earth System Sciences*, *27*(9), 1865–1889. https://doi.org/10.5194/hess-27-1865-2023

Stevens, B., Satoh, M., Auger, L., Biercamp, J., Bretherton, C. S., Chen, X., et al. (2019). DYAMOND: The dynamics of the atmospheric general circulation modeled on non-hydrostatic domains. *Progress in Earth and Planetary Science*, *6*(1), 61. https://doi.org/10.1186/s40645-019-0304-z

Takasuka, D., Becker, T., & Bao, J. (2025). Precipitation characteristics and thermodynamic-convection coupling in global kilometre-scale simulations. *Earth and Space Science Open Archive*.

Takasuka, D., Satoh, M., Miyakawa, T., Kodama, C., Klocke, D., Stevens, B., et al. (2024). A protocol and analysis of year-long simulations of global storm-resolving models and beyond. *Progress in Earth and Planetary Science*, *11*(1), 66. https://doi.org/10.1186/s40645-024-00668-1

Tao, C., Xie, S., Ma, H., Bechtold, P., Cui, Z., Vaillancourt, P. A., et al. (2024). Diurnal cycle of precipitation over the tropics and central United States: Intercomparison of general circulation models. *Quarterly Journal of the Royal Meteorological Society*, *150*(759), 911–936. https://doi.org/10.1002/qj.4629

Tomassini, L. (2025). Changes in clouds and the tropical circulation in global kilometer-scale simulations under different warming patterns. *Journal of Climate*, *38*(1), 57–86. https://doi.org/10.1175/jcli-d-24-0068.1

Tomassini, L., Willett, M., Sellar, A., Lock, A., Walters, D., Whitall, M., et al. (2023). Confronting the convective gray zone in the global configuration of the met office unified model. *Journal of Advances in Modeling Earth Systems*, *15*(5), e2022MS003418. https://doi.org/10.1029/2022ms003418

Wang, Y., Zhang, Y., Han, Y., Xue, W., Zhou, Y., Li, X., & Chen, H. (2025). *Global climate modeling with improved precipitation characteristics by learning physics (GRIST-MPS v1.0)*. EGUsphere.

Watters, D., Battaglia, A., & Allan, R. P. (2021). The diurnal cycle of precipitation according to multiple decades of global satellite observations, three CMIP6 models, and the ECMWF reanalysis. *Journal of Climate*, *34*(12), 5063–5080. https://doi.org/10.1175/jcli-d-20-0966.1

Yan, Z., Lu, X., Wu, L., Liu, F., Qiu, R., Cui, Y., & Ma, X. (2025). Evaluation of precipitation forecasting based on GraphCast over mainland China. *Scientific Reports*, *15*(1), 14771. https://doi.org/10.1038/s41598-025-98944-7

Yang, G.-Y., & Slingo, J. (2001). The diurnal cycle in the tropics. *Monthly Weather Review*, *129*(4), 784–801. https://doi.org/10.1175/1520-0493(2001)129<0784:tdcitt>2.0.co;2

Yang, S., & Smith, A. E. (2006). Mechanisms for diurnal variability of global tropical rainfall observed from TRMM. *Journal of Climate*, *19*(20), 5190–5226. https://doi.org/10.1175/jcli3883.1

Zhang, B., Donner, L., Zhao, M., & Tan, Z. (2024). Improved precipitation diurnal cycle in GFDL climate models with non-equilibrium convection. *Journal of Advances in Modeling Earth Systems*, *16*(9), e2024MS004315. https://doi.org/10.1029/2024ms004315

Zou, L., & Zhou, T. (2024). Convection-permitting simulations of current and future climates over the Tibetan Plateau. *Advances in Atmospheric Sciences*, *41*(10), 1901–1916. https://doi.org/10.1007/s00376-024-3277-9